



In Vivo Sustained Release of Peptide Vaccine Mediated by Dendritic Mesoporous Silica Nanocarriers

Weiteng An¹, Sira Defaus^{2*}, David Andreu² and Pilar Rivera-Gil^{1*}

¹ Integrative Biomedical Materials and Nanomedicine Laboratory, Department of Experimental and Health Sciences, Universitat Pompeu Fabra, Barcelona, Spain, ² Proteomics and Protein Chemistry Unit, Department of Experimental and Health Sciences, Universitat Pompeu Fabra, Barcelona, Spain

OPEN ACCESS

Edited by:

David Pozo,
University of Seville, Spain

Reviewed by:

Even Fossum,
Oslo University Hospital, Norway
Xin Li,
China Agricultural University, China

*Correspondence:

Pilar Rivera-Gil
pilar.rivera@upf.edu
Sira Defaus
sira.defaus@upf.edu

Specialty section:

This article was submitted to
Molecular Innate Immunity,
a section of the journal
Frontiers in Immunology

Received: 23 March 2021

Accepted: 24 May 2021

Published: 16 June 2021

Citation:

An W, Defaus S, Andreu D and
Rivera-Gil P (2021) In Vivo
Sustained Release of Peptide
Vaccine Mediated by
Dendritic Mesoporous
Silica Nanocarriers.
Front. Immunol. 12:684612.
doi: 10.3389/fimmu.2021.684612

Mesoporous silica nanoparticles have drawn increasing attention as promising candidates in vaccine delivery. Previous studies evaluating silica-based vaccine delivery systems concentrated largely on macromolecular antigens, such as inactivated whole viruses. In this study, we synthesized dendritic mesoporous silica nanoparticles (DMSNs), and we evaluated their effectiveness as delivery platforms for peptide-based subunit vaccines. We encapsulated and tested *in vivo* an earlier reported foot-and-mouth disease virus (FMDV) peptide vaccine (B₂T). The B₂T@DMSNs formulation contained the peptide vaccine and the DMSNs without further need of other compounds neither adjuvants nor emulsions. We measured *in vitro* a sustained release up to 930 h. B₂T@DMSNs-57 and B₂T@DMSNs-156 released 23.7% (135 µg) and 22.8% (132 µg) of the total B₂T. The formation of a corona of serum proteins around the DMSNs increased the B₂T release up to 61% (348 µg/mg) and 80% (464 µg/mg) for B₂T@DMSNs-57 and B₂T@DMSNs-156. *In vitro* results point out to a longer sustained release, assisted by the formation of a protein corona around DMSNs, compared to the reference formulation (i.e., B₂T emulsified in Montanide). We further confirmed *in vivo* immunogenicity of B₂T@DMSNs in a particle size-dependent manner. Since B₂T@DMSNs elicited specific immune responses in mice with high IgG production like the reference B₂T@Montanide™, self-adjuvant properties of the DMSNs could be ascribed. Our results display DMSNs as efficacious nanocarriers for peptide-based vaccine administration.

Keywords: dendritic mesoporous silica nanoparticles, peptide vaccines, sustained and controlled release, foot-and-mouth disease virus, nanovaccine, immunogenicity, adjuvancy

INTRODUCTION

Peptide-based vaccines are considered an attractive alternative strategy to overcome many of the limitations of conventional (inactivated, attenuated) whole virus-based vaccines (1–3). They present advantages such as reduced toxicity, good definition of T- and B-cell epitopes for targeted immune responses, cost-effective scale up manufacturing processes, easy handling, storage, and transport (1, 4, 5). These advantages have prompted the progress of many peptide-based vaccines to different preclinical and clinical stages (1, 6, 7). Nevertheless, peptide-based vaccines tend to be poorly

immunogenic usually requiring adjuvants, multivalency, and/or delivery systems to become more effective *in vivo*. Adjuvants of different kinds, such as aluminum hydroxide, mineral salts, water-oil emulsions, or liposome-based formulations have been developed to enhance efficacy (7). Although these strategies can boost to a certain extent the low immunogenicity of peptide-based vaccines, only a limited number are approved for human and animal applications due to their not well-established mode of action, as well as to other related toxicity and safety issues (8, 9).

In the last decade, the field of nanovaccines has gained maturity (10–13). Nanoparticles, especially synthetic ones made of polymers, phospholipids, metal, carbon, or silica (14) among other compositions have been extensively studied for vaccine applications ref (1, 9, 15, 16). Within the variety of nanomaterials used for vaccine delivery, mesoporous silica nanoparticles (MSNs), especially dendritic mesoporous silica nanoparticles (DMSNs), are emerging as promising vaccine delivery platforms because of their versatile formulation, boosting abilities, lack of side effects, and depot effect. They have unique central-radial pore structures with large pore sizes (17–19) and are characterized by low cross-linking silica frameworks with fast degradability rate *in vivo* (20). Studies on DMSNs show their enhanced loading capacity, sustained release profile, easy surface functionalization, and potential adjuvant activity (21, 22). Furthermore, DMSNs have shown effective immune potentiation *in vivo*, inducing strong humoral and cellular immune responses against target antigens (23–25). The majority of studies on MSNs-based vaccine delivery systems are focused on carrying large-size immunogens, such as bacterial recombinants, viral capsid proteins and OVA- and BSA-conjugated model vaccines (26–29), whereas few papers explore their use to carry smaller biomolecules, such as peptides in subunit vaccines.

In this study, we extend the use of DMSNs to delivery platforms for peptide-based vaccines and evaluate their *in vivo* effectiveness. We have encapsulated a peptide construct named B₂T, which confers full protection against foot-and-mouth disease virus (FMDV) in swine (30, 31). Previous publications of the authors have shown that inclusion of a T-cell epitope in the B₂T construct provides a rather powerful T-cell response (lymphoproliferation, γ -interferon production) (31–33). B₂T is currently administered emulsified with Montanide™ ISA 50V2 W/O (water in oil) (*i.e.*, B₂T@Montanide™). This formulation has some drawbacks. For instance, there are several studies reporting unacceptable local reactions toward the Montanide adjuvant (34). Moreover, Montanide requires a dedicated emulsification procedure for each antigen which add complexity to its industrial production (35). To overcome these challenges, we have explored the use of DMSNs loaded with B₂T as nanovaccine against FMDV. Briefly, we have synthesized DMSNs of different sizes (57 ± 9 nm and 156 ± 10 nm) and have loaded them with B₂T, naming the resulting nanoformulation B₂T@DMSNs. Both sizes exhibited high B₂T loading capacities (570 μ g/mg for DMSNs-57 and 580 μ g/mg for

DMSNs-156) and an *in vitro* sustained B₂T release profile over 930 h. Furthermore, RAW 264.7 macrophage cells efficiently internalized the fluorescent version of both nanoformulations in a size-dependent manner. Finally, we have confirmed a specific immune response with high IgG production upon vaccination of outbred Swiss mice (Swiss ICR-CD1) with two doses of B₂T@DMSNs, obtaining similar antibody titers than those elicited by the previous gold standard B₂T@Montanide™.

MATERIALS AND METHODS

For a detailed description of the procedures and more results, we refer the readers to the **Supporting Information File**.

Synthesis and Characterization of DMSNs-57 and DMSNs-156

The DMSNs with a diameter of 156 nm (designated as DMSNs-156) were synthesized using a modified version of a previously reported method (17). Briefly, 136 mg TEA were added to 50 mL Milli-Q water and stirred at 500 rpm, 80°C for 0.5 h. Then, 760 mg CTAB and 250 mg sodium salicylate (NaSal) was added to the above solution and stirred for another 1 h. Next, 4 ml TEOS was added dropwise to the solution under stirring, which continued overnight. The products were collected by centrifugation at 12,000 rpm for 10 min and washed three times with ethanol. Then, the collected products were extracted three times with 80 ml of methanol solution containing 4.5 ml of HCl (37%) at 65°C for 6 h to remove the template. Finally, the nanoparticles were dried in vacuum at room temperature overnight. DMSNs with a diameter of 57 nm (designated as DMSNs-57) were synthesized following the abovementioned method except for decreasing the amount of structure directing agent NaSal from 250 to 83 mg.

The structure of both DMSNs types was imaged with a transmission electron microscope (TEM, JEOL JEM1010) at an acceleration voltage of 80 kV. TEM specimens were prepared by evaporating one drop of ethanolic nanoparticle solution on Ted Pella Formvar carbon-coated copper grids. The z-potential and hydrodynamic diameter of the samples was determined in a Malvern Zetasizer ZS instrument at 25°C. Samples were dispersed in water and transferred into disposable polystyrene cuvette. The given values are the average of triplicate readings.

See de **Supplementary File** (section §SI-1.1) for complementary information.

B₂T Synthesis

The dendrimeric B₂T immunogen was produced as described earlier (31), by conjugation of 2 copies of the B-cell epitope moiety to a maleimide-functionalized T-cell epitope. The conjugation reaction was clean and practically quantitative, and the resulting branched peptide was satisfactorily characterized by HPLC and mass spectrometry. See section §SI-1.2 for complementary information and section §SI-2.1 for the synthesis of fluoro-B₂T@DMSNs.

B₂T Loading in DMSNs-57 and DMSNs-156 and Quantification of Peptide Loading

We followed the same methodology to load B₂T into both DMSNs sizes. The resulting products were named, B₂T@DMSNs-57 and B₂T@DMSNs-156. Briefly, 1.5 mg B₂T and 2.0 mg DMSNs were mixed in 2.0 mL DPBS buffer solution (pH 7.4) and then properly dispersed by sonication for 5 min. The resulting mixture was gently shaken at 200 rpm for 5 h at RT. Afterward, the products were separated by centrifugation at 12,000 rpm for 10 min and washed twice with PBS. B₂T encapsulation efficiency (EE%) was defined as follows:

$$B_2T \text{ encapsulation efficiency (EE \%)} \\ = (\text{weight of loaded } B_2T / \text{weight of total } B_2T) \times 100 \%$$

where the amount of loaded B₂T was determined by subtracting the free B₂T in the supernatant from the total amount, and the amount of free B₂T in the supernatant was calculated based on the B₂T calibration curve obtained in DPBS (section §SI-1.3, **Figure SI-3**). See section §SI-1.4 for complementary information on the impact of key parameters (ionic strength, peptide structure, and DMSNs charge) on the loading efficiencies, and section §SI-2.1 for the loading of fluoro-B₂T into DMSNs.

B₂T Calibration Curve

A B₂T stock solution (1,000 µg/ml) was prepared by dissolving 2 mg lyophilized B₂T powder in 2 ml DPBS. From this stock solution serial dilutions in DPBS (31.3, 62.5, 125, 250, and 500 µg/ml) were prepared and measured on a BiochromTM Ultrospec 2100 Pro UV/Vis spectrophotometer using a quartz cuvette with a 1-cm path length (with DPBS as blank). The calibration curve was constructed by plotting the absorbance at 225 nm against the corresponding B₂T concentrations. See section §SI-1.3 for complementary information.

B₂T Release Kinetics From the DMSNs

Release experiments were carried out in 1.5 ml Eppendorf tubes containing 1.0 mg DMSNs loaded with B₂T and 1.0 ml DPBS (pH 7.4). Samples were gently shaken at 37°C and, at predetermined time points, the suspension was centrifuged at 12,000 rpm for 10 min. We took the supernatant and measure the absorbance (225 nm) of B₂T released. The procedure was repeated for each time point and for both DMSNs. Fresh DPBS (same volume than aliquot of supernatant taken) was added to redisperse the pellet. All release measurements were performed in duplicate.

Imaging the Cellular Uptake of B₂T@DMSNs

RAW 264.7 cells in RPMI 1640 medium (containing 2 mM L-glutamine, 10% heat-inactivated FBS, and 1% penicillin and streptomycin) were seeded in Ibidi µ-slide 8 well at a density of 5.0×10^4 cells/well. Cells were incubated at 37°C in an atmosphere of 5% CO₂ for 24 h. Then, 30 µg/ml of fluoro-B₂T@DMSNs was added to the cells. Following 0.5, 1, 2, 4, 8, and 16 h incubation, cells were washed three times with PBS, and

fresh growth medium containing CellMask deep red plasma membrane was added and incubated for 8 min. After three washes with PBS, fresh PBS was added, and cells were imaged by confocal laser scanning microscopy (CLSM). See section §SI-2.2 for complementary information.

Flow Cytometry Analysis of Cellular Uptake

RAW 264.7 cells were seeded in six-well plates in RPMI 1640 medium (containing 2 mM L-glutamine, 10% heat-inactivated FBS, and 1% penicillin and streptomycin) at a density of 1.0×10^6 cells/well. Cells were incubated at 37°C in an atmosphere of 5% CO₂ for 24 h. Then, 30 µg/ml fluoro-B₂T@DMSNs was added. Following 0.5, 1, 2, 4, 8, and 16 h incubation, cells were washed three times with PBS, new PBS was added, and cells were carefully detached from the plates with a Falcon cell scraper. The collected cells were transferred to tubes, were placed in ice, and the nuclear dye, DAPI was added to a final concentration of 1.0 µg/ml, and incubated for 2 min. The labelled cells were then measured by flow cytometry (FC) in a BD LSRFortessa X-50 flow cytometer. The mean fluorescence intensity (MFI) and percentage of cells with a positive fluorescent signal compared to the control (untreated cells) were determined on 5,000 gated single-living cells. FACS data were processed by the method described in section §SI-2.3.

Mice Immunization

Experiments were carried out in the animal facility of the CSIC Center for Research and Development (CID-CSIC), in agreement with EU (Directive 2010/63/EU on the protection of animals used for scientific purposes) and domestic (Real Decreto 53/2013) regulations. The protocol to produce antibodies was in accordance with institutional guidelines under a license from the local government (DAAM 7463) and was approved by the Institutional Animal Care and Use Committee at the CID-CSIC.

All formulations were prepared on the day of injection. Mice were randomized into groups and inoculated by two subcutaneous injections over the interscapular area at day 0 and day 21. All mice were euthanized at day 40 by carbon dioxide inhalation. Animals were monitored three times per week for health during the study.

To assess immunogenicity of B₂T@DMSNs in mice, two trials were performed (section §SI-3). In the first one, mice were divided into three groups as shown in **Table SI-1**. The first group was the positive control group (4 mice) which was immunized with 200 µl of Montanide ISA 50V2 emulsion containing 100 µg B₂T (B₂T@MontanideTM), following earlier studies (30); the second (six mice) and third (four mice) groups were the sample groups. The second group was treated with 100 µg B₂T loaded in DMSNs-156 (B₂T@DMSNs-156) in 200 µl DPBS, and the third group was treated with the same amount of DMSNs alone (163 µg DMSNs-156) in 200 µl DPBS. All groups were boosted at day 21. Blood samples were collected before vaccination (day 0) and at days 14, 20 (pre-boost), and 40 (euthanize, sample obtained by cardiac puncture). In the second trial, aimed at assessing the impact of DMSNs size on

mice immunization, mice were divided into three groups as shown in **Table SI-2**. The first group was again the positive control group (B₂T@Montanide™; three mice). The second (five mice) group was treated with the formulation B₂T@DMSNs-57 and the third (five mice) group with B₂T@DMSNs-156. All mice were treated with the same dose of peptide vaccine (100 µg B₂T). Blood sample collection was extended until day 80, to study the long-term immune effect of B₂T@DMSNs.

Detection of Specific Anti-B₂T Antibodies by ELISA

Specific antibodies were detected by enzyme-linked immunosorbent assay (ELISA). 96-well Costar® plates were coated with 50 µl B₂T (15.4 µg/ml) in bicarbonate/carbonate coating buffer (0.05 M, pH 9.6) and incubated at 4°C overnight. After washing three times with DPBS, 50 µl of diluted serums (two-fold dilution series of each collected serum sample were prepared, starting at 1/150, and each dilution sample in duplicate) were incubated for 1 h at 37°C, followed by four DPBS washes. Pre-immune sera from mice were used as negative controls. Next, 50 µl of a 1:4,000 dilution of HRP-labeled rabbit anti-mouse IgG were added and incubated for 1 h at 37°C followed by five washings with DPBS. Then, 100 µl of TMB substrate solution was added for 20 min at RT in the dark. Finally, the reaction was stopped by adding 100 µl of 1 M H₂SO₄. The optical density (OD) of the samples was measured in an ELISA reader (BioRad, CA, USA) at 450 nm. Titers in a log₁₀ scale were expressed as the reciprocal of the last dilution giving the absorbance recorded in the control wells (serum at day 0) plus 2 SD. See section §SI-3.2 for complementary information on the individual response of each mice to the treatment.

Statistical Analysis

Differences among B₂T@DMSNs-immunized groups in B₂T-antibody titers were analyzed by one-way ANOVA, followed by Tukey's post-hoc comparisons tests. Values are cited in the text as means ± SD. All *p* values are two-sided, and *p* values < 0.05 were considered significant. Statistical analyses were conducted using GraphPad Prism Software 5.0 (San Diego, CA, USA).

RESULTS

DMSNs Synthesis and Physicochemical Characterization

TEM measurements showed that both types of DMSNs have an inorganic core diameter of 57 ± 9 nm (DMSNs-57) and 156 ± 10 nm (DMSNs-156) (**Figure 1A, B**; §SI-1.1, **Figures SI-1A–D**). DLS measurements indicated that the averaged hydrodynamic diameter of DMSNs-57 was 75 nm with a polydispersity index (PDI) of 0.060 and the averaged hydrodynamic diameter of DMSNs-156 was 227 nm with a PDI of 0.061 (**Figure 1C**; §SI-1.1, **Figure SI-1.E**). The low PDIs for both nanoparticles demonstrate excellent monodispersity and uniformity which are consistent with TEM images. As expected, the DLS

measurement showed higher size values for the DMSNs than those measured by TEM. This is due to the DMSNs' surface hydration in aqueous solution (36). The z-potential values of DMSNs-57 and DMSNs-156 were -30.2 mV and -37.1 mV, respectively (**Figure 1C**). These results indicate colloidal stability and homogenous size distribution.

Loading B₂T Vaccine Into Differently Sized DMSNs (B₂T@DMSNs) and *In Vitro* Characterization of B₂T Release Kinetics

After synthesizing DMSNs-57 and DMSNs-156, we performed their loading with the B₂T peptide vaccine (see section §SI-1.2, **Figure SI-2** for B₂T structure). The B₂T amount loaded into both types of DMSNs was quantified based on its absorbance at 225 nm (section §SI-1.3, **Figure SI-3A**) and using a calibration curve (section §SI-1.3, **Figure SI-3B**). We quantified 1.14 mg and 1.16 mg of B₂T loaded in 2.0 mg of DMSNs-57 and DMSNs-156, respectively. The loading capacities were 570 µg/mg DMSNs for DMSNs-57 and 580 µg/mg DMSNs for DMSNs-156, and the encapsulation efficiencies (EE%) reached 76% and 77%, respectively. Regardless the differences in DMSNs sizes, we measured similar loading efficiencies. We attribute this to their close z-potential values and to the equivalent hydrogen bonds and polar interactions with the peptide (37). The high B₂T loading capacities obtained are probably related to the strong electrostatic interaction between the anionic DMSNs and the positively charged B₂T (pI 10.88) in DPBS (pH 7.4) and to the DMSNs central-radial pore structures with large surface areas (17, 18).

We performed the loading under different conditions (section §SI-1.4) (38, 39) to evaluate the impact of ionic strength (**Figure SI-4**), peptide (cargo) structure (dendrimer vs. linear) (**Figure SI-5**) and DMSNs charge (**Figure SI-6**) on the loading efficiency of the DMSNs. We used, for comparison, 168 nm solid silica nanoparticles (SNSs-168) (**Figures SI-4 and SI-5**). Results on section §SI-1.4 (**Figures SI-4, SI-5, SI-6**) displayed that the higher the ionic strength, the more B₂T was loaded into all silica nanoparticles. Being DMSNs more efficient than SNSs. The trend was maintained for the dendrimer B₂T and a linear control peptide (O PanAsia B epitope B) regardless of DMSNs charge. Up to 5× ionic strength, DMSNs-156 were more efficiently loading the peptide. Note that within this work the ionic strength was set at 1×. Furthermore, we observed that our synthesized, negatively charged DMSNs were significantly more effective in loading the B₂T peptide than their positively charged counterparts (**Figure SI-6**).

Next, we investigated the B₂T release kinetics from the DMSNs. To this end B₂T@DMSNs were dispersed in a saline buffer (1× DPBS). At given time points, we collected the supernatants after centrifugation, we measured their absorbance at 225 nm and with help of the calibration curve (**Figure SI-3.B**), we quantified the amount of B₂T released from the DMSNs. **Figure 2** shows a sustained release of B₂T up to 1000 h (41 days). After 700 h, the release curve reached a plateau. Both B₂T@DMSNs-57 and B₂T@DMSNs-156 showed similar release kinetics. The B₂T amount released in B₂T@DMSNs-57

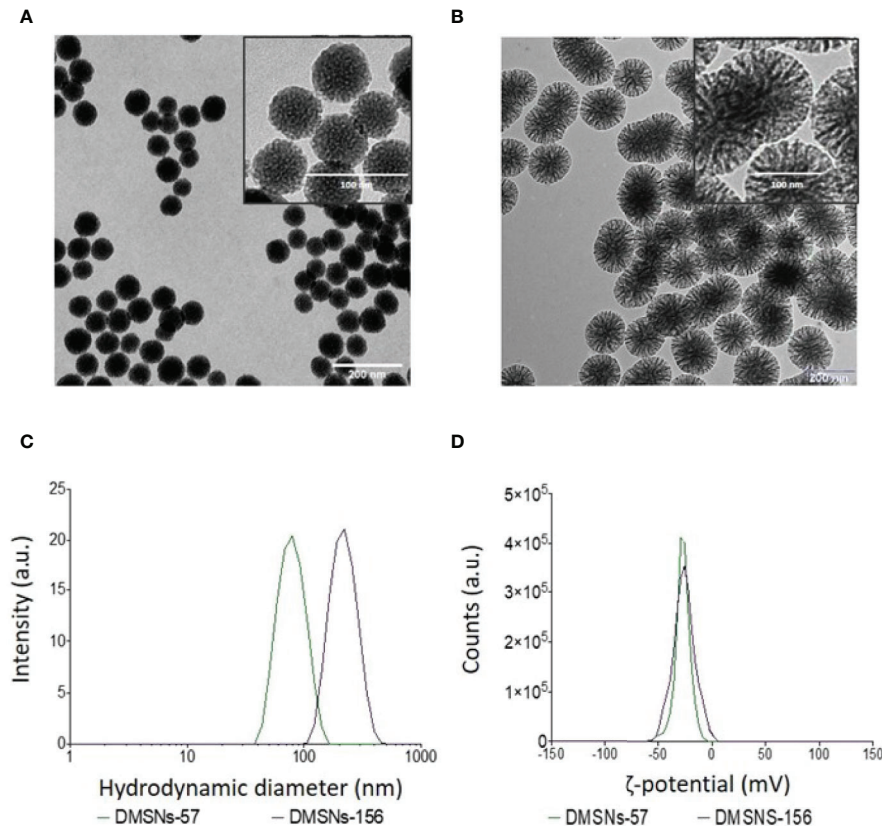


FIGURE 1 | TEM and DLS analysis of DMSNs-57 and DMSNs-156. TEM image of 57 nm DMSNs (A) and of 156 nm DMSNs (B). Scale bar, 200 nm. The insets show the DMSNs with higher magnification revealing the dendritic structure. Scale bar, 100 nm. (C) DMSNs-57 and DMSNs-156 hydrodynamic size (75 ± 9 nm and 156 ± 10 nm) and (D) ζ -potential values (-30.2 and -37.1 mV).

and B₂T@DMSNs-156 corresponds to 23.7% (135 μ g) and 22.8% (132 μ g) of the total amount loaded.

Albumin is one of the most frequent proteins in physiological fluids and a major component of the protein corona of biomedical nanomaterials dispersed in such fluids (40–44). It is also known that the protein corona formed on nanoparticles is a dynamic system. Following typical nanoparticle behavior, we expected a protein corona around our DMSNs upon their *in vivo* administration. We therefore wanted to elucidate the impact of the protein corona on the B₂T release kinetics (Figure 2). To this end, we dispersed the B₂T@DMSNs in medium containing albumin (BSA 250 μ g/ml in DPBS), allowed the DMSNs to build their protein corona and measured the B₂T release (section §SI-1.5) following the procedure described before. We took advantage of the distinct absorption peaks for B₂T at 225 nm (section §SI-1.3) and for albumin at 280 nm (section §SI-1.5, Figure SI-7) to build calibration curves. In this case we could also track changes on the protein corona formed around the B₂T@DMSNs. Our methodology enabled the concomitant quantification of the release of both components, B₂T and albumin, from the DMSNs to the medium. We validated this technology with HPLC (section §SI-1.5, Figure SI-8). Then we

quantified the B₂T release from the protein coated DMSNs (Figure 2) and correlated the results with the amount of albumin released from the protein corona (section §SI-1.5, Figure SI-9).

After the formation of the protein corona, B₂T release increased 158% on B₂T@DMSNs-57 and 252% on B₂T@DMSNs-156. This corresponds to 61% (348 μ g/mg) and 80% (464 μ g/mg) of the total B₂T loaded within B₂T@DMSNs-57 and B₂T@DMSNs-156, respectively. It seems evident, that the presence of BSA significantly enhances B₂T release. We ascribed this effect to a competitive interaction towards the DMSNs in favor of BSA resulting in B₂T displacement and release (45, 46). To prove this, we monitored the changes of BSA concentration in the dispersed medium in the presence of the DMSNs (Figure SI-9). As seen in Figure SI-9, during the first 66.5 hours, both B₂T@DMSNs-57 and B₂T@DMSNs-156 kept absorbing BSA from the medium, probably due to forming BSA protein corona on DMSNs, which resulted in lower BSA concentrations (< 250 μ g/mL) in the supernatants. Afterwards, the BSA level in both formations kept fluctuating around 250 μ g/ml (initial concentration added) which points out to an absence of protein corona around the DMSNs. Although longer

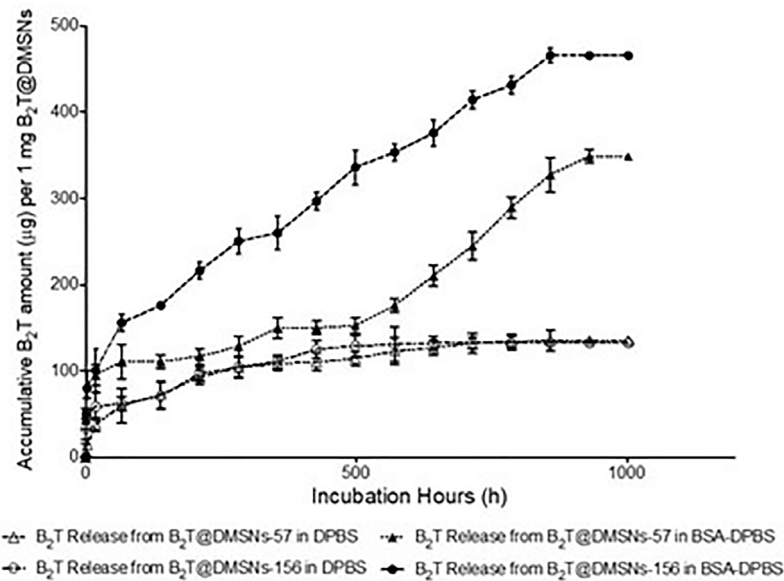


FIGURE 2 | B₂T release profiles from B₂T@DMSNs-57 and from B₂T@DMSNs-156 dispersed in DPBS or BSA-DPBS. After each time point, the supernatants were collected for UV-vis analysis and the pellets were redispersed in the same volume of medium. The procedure was repeated during 1,000 h.

experiments would be required to draw a conclusion, these results may indicate a long-term sustained release promoted by the DMSNs. At any rate, they confirm vaccine release from the DMSNs in physiological complex media as the one in the cell.

Internalization of B₂T@DMSNs by Macrophages

Cellular uptake of antigens by innate immune cells provides antigen-processing and subsequent costimulatory signals that are crucial to trigger acquired immune responses, especially for low immunogenic peptide antigens. Macrophage-like RAW 264.7 cells (47) are often used to study cellular responses to microbes and their products (48). We selected this cell model to assess *in vitro* cellular internalization of our nanoformulations, using 1 mg DMSNs-57 and 1 mg DMSNs-156 loaded with 200 µg B₂T labeled with a dye (*i.e.*, fluoro-B₂T) (see section §SI-2 and **Figure SI-10**). Similar to other nanoparticles (49), cellular uptake of fluoro-B₂T@DMSNs occurred in a size-dependent manner (**Figure 3**). The maximum uptake level was observed after 4 h for the fluoro-B₂T@DMSNs-57 (57 nm size) and after 8 h for the fluoro-B₂T@DMSNs-156 (156 nm size) (**Figures 3A, B**, and §SI-2 and **Figures SI-11, SI-12 and SI-13**). During the first 4 h, the amount of B₂T@DMSNs-57 interacting with the cells was approximately two times the amount of B₂T@DMSNs-156 (**Figure 3B**). We can conclude that at least after an acute exposure, the smaller DMSNs-57 are faster internalized by RAW 264.7 cells than larger DMSNs-156. It is noteworthy that after the cellular uptake reached the maximum value, longer incubation times resulted in reduced uptake values. We suppose that it is due to the fast cell growth and division of RAW 264.7 cells (50) which resulted in the “dilution effect” of fluorescence intensity per cell.

Sustained Mice Immunogenicity Provided by B₂T@DMSNs

We next validated B₂T@DMSNs performance by testing *in vivo* their immunogenicity. To this end, we performed two sets of vaccination trials in mice (see section §SI-3 for a detailed description). In both trials, we injected subcutaneously samples containing the same amount of B₂T antigen (100 µg) at day 0 and boosted with the same dose at day 21. We performed an ELISA to detect specific anti-B₂T antibodies in sera collected following the schedule shown in **Tables SI-1 and SI-2** (section §SI-2). In the first trial (**Table SI-1 and Figure 4**), mice were vaccinated with B₂T@MontanideTM (positive control), B₂T@DMSNs-156, and bare DMSNs-156 (negative control). Results in **Figure 4** show that B₂T@DMSNs treatment elicits a consistent response with all treated mice, presenting an increase in anti-B₂T IgG production values after the boost (day 40). Although the anti-B₂T IgG level from B₂T@DMSNs-156 is slightly lower than B₂T@Montanide, these results confirm that B₂T@DMSNs-156 successfully stimulates anti-B₂T-specific immune response in mice. On the contrary, as expected, no enhancement of the immune response was found in mice treated with bare DMSNs-156.

Once we confirmed the immunogenic effect of B₂T@DMSNs and considering their long-time sustained release profile obtained *in vitro* (**Figure 2**), we performed a second trial (section §SI-2, **Table SI-2**). In this case, mice vaccinated with either B₂T@DMSNs-57 or B₂T@DMSNs-156 particle sizes were subjected to a longitudinal analysis of serum-IgG responses up to 80 days. As shown in **Figure 5**, anti-B₂T IgG titers were clearly boosted up among all tested formulations at day 40, although this time we also detected serum-IgG responses in some mice

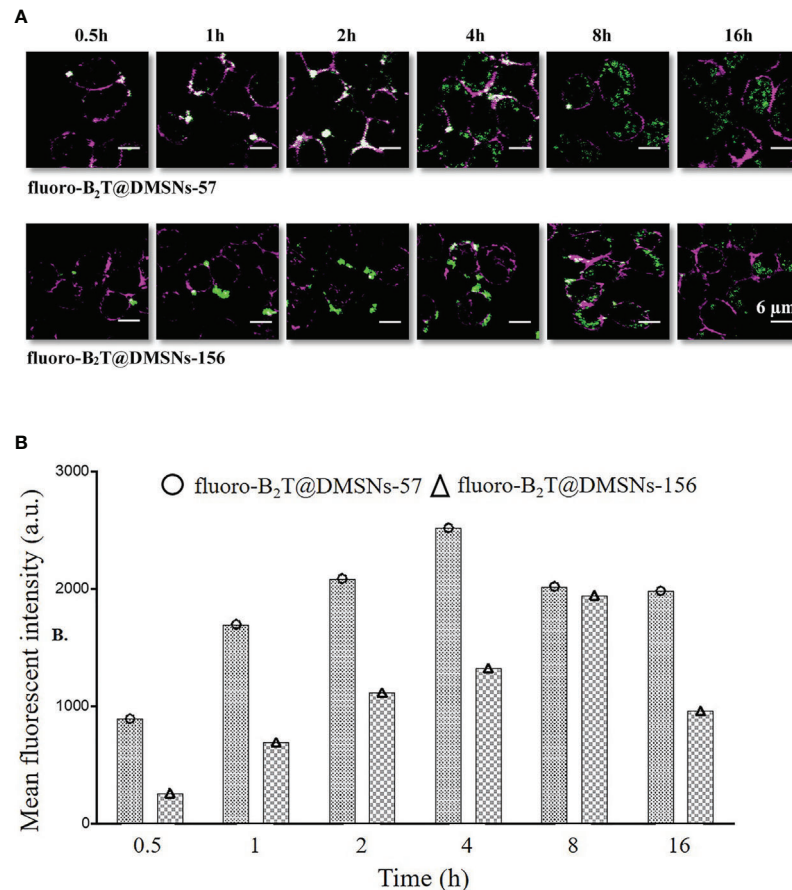


FIGURE 3 | RAW 264.7 macrophage cellular interactions of fluoro-B₂T@DMSNs-57 and fluoro-B₂T@DMSNs-156. **(A)** CLSM images showing a time- and DMSNs size-dependent internalization. (Note: Green correspond to BodiFluor-488 conjugated to the B₂T loaded within the DMSNs whereas the magenta color corresponds to the dye, cell mask deep red used to stain the plasma membrane of the cells). (cf. §SI-11, **Figures SI-11, SI-12, and SI-16**) **(B)** Flow cytometry analysis of cellular interactions. The columns represent the mean fluorescence intensity of fluoro-B₂T@DMSNs-57 and fluoro-B₂T@DMSNs-156. (cf. §SI-2.3, **Figures SI-13**).

immunized with B₂T@DMSNs-156 already at day 20 before the boost. We do not have a clear explanation for these different results between trials, so we attribute it to the intrinsic variability of *in vivo* studies (section §SI-3, **Figures SI-14, SI-15, and SI-16**). B₂T@DMSNs-57 and B₂T@DMSNs-156 showed slightly lower post-boosting titers than the positive control, B₂T@Montanide™. However, in the case of the B₂T@DMSNs-57 mice group, their serum titers increased over time until reaching comparable IgG levels to the positive control group at days 60 and 80 with high consistency among individuals. These results with the DMSNs-57 formulation are in consonance with published works reporting nanoparticle traffic to the draining lymph node in a size-dependent manner, with small 20–50 nm nanoparticles being more efficiently drained than bigger ones (9, 23, 25). We can confirm the efficiency of DMSNs to induce sustained Ab responses in a size dependent manner comparable to the emulsified version B₂T@Montanide™, pointing to demonstrable adjuvant properties of DMSNs. Finally, it is worth noting that, as not all B₂T is released from the DMSNs

at day 80, one could possibly expect a sustained immunogenic effect beyond that time point.

CONCLUSIONS

Biopharmaceutical companies are now actively focused on the development of sustained release drug delivery systems, in view of their inherent benefits. Sustained release formulations designed to maintain the required therapeutic concentrations over an extended period of time present several advantages over conventional dosage forms, including less frequent drug dose, reduced concentration fluctuations, minimal side effects, reduced healthcare costs, improved efficiency and/or immune responses (51, 52). In this context, DMSNs are gaining increasing interest as effective delivery system because they are tunable, exhibit high loading capacity for therapeutic agents, and their release can be controlled. In this work, we evaluate the applicability of these nanocarriers in vaccination and long-term protection using a peptide-based vaccine with

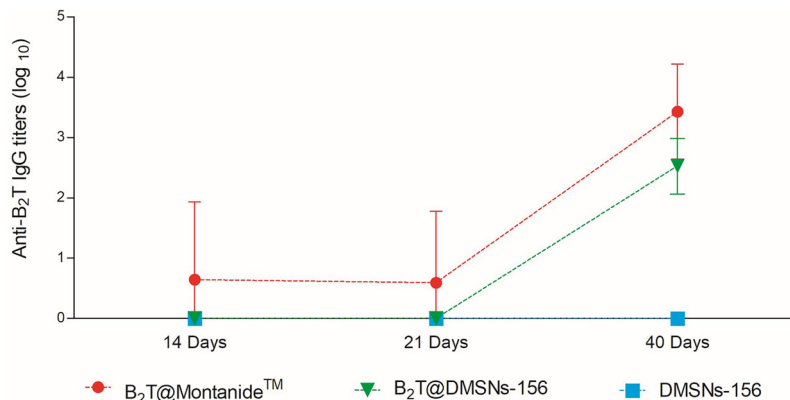


FIGURE 4 | *In vivo* functional validation. ELISA-determined anti-B₂T peptide responses of mice vaccinated with B₂T@Montanide™ (red circle, n=4), B₂T@DMSNs-156nm (green down triangle, n=6), DMSNs-156nm (blue squares, n=4) from sera collected at days 14, 21 (pre-boost) and 40 (post-boost) post-immunization. Each point depicts mean antibody titers (calculated as described in Materials and methods) ± SD for each group. No individual spontaneous reactivity was observed in the titers determined at day 0. (cf. §SI-3; **Table SI-1**, and **Figures SI-14**, **SI-15**, and **SI-16**).

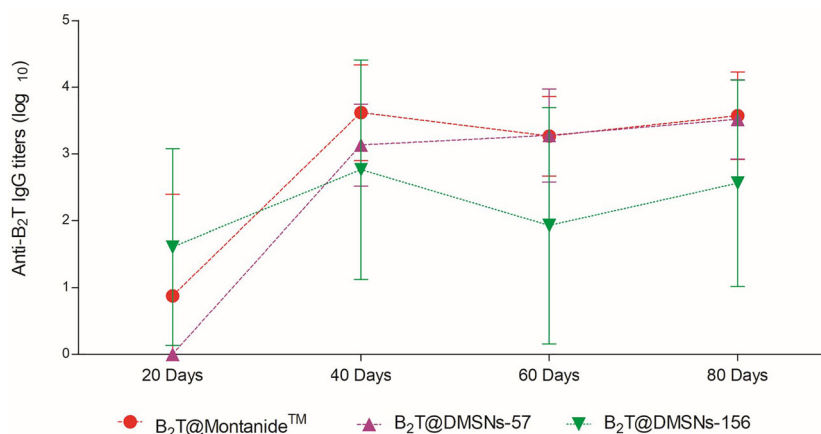


FIGURE 5 | Sustained *in vivo* immune response performed by the DMSNs. ELISA-determined anti-B₂T peptide responses obtained in vaccination trial II (**Table SI-2**) of mice vaccinated with B₂T@Montanide™ (red circle, n=3), B₂T@DMSNs-57nm (purple up triangle, n=5) and B₂T@DMSNs-156nm (green down triangle, n=5) from sera collected on the indicated days post-immunization (20, 40, 60, and 80 p). Each point depicts mean antibody titers (calculated as described in Materials and methods) ± SD for each group. No individual spontaneous reactivity was observed in the titers determined at day 0. (cf. §SI-3; **Table SI-2**, and **Figures SI-14**, **SI-15**, and **SI-16**).

previously reported protective immunity against FMDV. Our results demonstrate that DMSNs are colloidal stable and monodisperse, with high loading capacities for a bioactive peptide such as B₂T, besides being reported as non-toxic (53–56). The B₂T@DMSNs resulting formulations present long-term sustained *in vitro* release properties, enhanced in the presence of BSA. Tracking a fluoro-labeled version of B₂T within DMSNs formulations we could observe acute differences (within 16 h) in the internalization of the B₂T@DMSNs by macrophage cells in a size dependent manner. Finally, the effectivity of B₂T@DMSNs as nanovaccine was validated *in vivo* by comparing the immunogenic response to that of the positive control B₂T@Montanide™. Mice vaccination trials showed

that both DMSNs formulations increased specific B₂T antibody titers in a similar manner. However, results revealed a trend toward higher antibody titers in the animal group immunized with DMSNs of smaller particle size (57 nm) in agreement with previous literature (57, 58). Taken together, these results indicate that DMSNs is an excellent carrier for peptide vaccine which favors the internalization of the antigen by immune cell. Besides, they also delay or slow down their *in vivo* release, finally leading to a long-lasting sustained immune response activation. Therefore, DMSNs may be a suitable vaccine delivery system alternative to conventional adjuvanted vaccines not only for whole viruses or protein antigens but also for synthetic peptide-based subunit candidates.

DATA AVAILABILITY STATEMENT

The original contributions presented in the study are included in the article/**Supplementary Material**. Further inquiries can be directed to the corresponding author.

ETHICS STATEMENT

The animal study was reviewed and approved by DAAM 7463.

AUTHOR CONTRIBUTIONS

WA contributed to the design of the synthesis study, to data analysis, and wrote the first draft. SD contributed to the design of the *in vivo* study, and to its data analysis. DA contributed to the design of the *in vivo* study. PR contributed to the conception and design of the study, to data analysis and wrote the manuscript. All authors contributed to the article and approved the submitted version.

FUNDING

This research was funded by Spanish Ministry of Science, Innovation and Universities (grants AGL2014-48923-C2 and

AGL2017-84097-C2-2-R to DA) as well as by Generalitat de Catalunya (grant 2009SGR492 to DA).

ACKNOWLEDGMENTS

PRG acknowledges The Generalitat de Catalunya (2017SGR 1054 - AGAUR) and the Ministry of Science, Innovation and Universities (MICINN) and the AEI (AEI-PID2019-106755RB-I00, RYC-2012-10059, MDM-2014-0370-04, CTQ2013-45433-P [FEDER], MAT2016-75362-C3-2-R, AEI-SAF2015-73052-EXP) for financial support. PR and WA thank the China Scholarship Council (201694910800) for the PhD fellowship of WA. The ICTS “NANOBIOSIS”, and particularly the Custom Antibody Service (CAbs, IQAC-CSIC, CIBER-BBN), is acknowledged for the assistance and support on animal experiments. We thank the UPF/CRG Flow Cytometry Unit (PRBB, Barcelona) for help with the flow cytometry analysis.

SUPPLEMENTARY MATERIAL

The Supplementary Material for this article can be found online at: <https://www.frontiersin.org/articles/10.3389/fimmu.2021.684612/full#supplementary-material>

REFERENCES

- Li W, Joshi MD, Singhania S, Ramsey KH, Murthy AK. Peptide Vaccine: Progress and Challenges. *Vaccines* (2014) 2:515–36. doi: 10.3390/vaccines2030515
- Fujita Y, Taguchi H. *Nanoparticle-Based Peptide Vaccines*. Oxford, United Kingdom; Cambridge, MA: William Andrew is an imprint of Elsevier (2017). doi: 10.1016/B978-0-323-39981-4.00008-7
- Moynihan KD, Holden RL, Mehta NK, Wang C, Karver MR, Dinter J, et al. Enhancement of Peptide Vaccine Immunogenicity by Increasing Lymphatic Drainage and Boosting Serum Stability. *Cancer Immunol Res* (2018) 6(9):1025–38. doi: 10.1158/2326-6066.CIR-17-0607
- Sesardic D. Synthetic Peptide Vaccines. *J Med Microbiol* (1993) 39:241–2. doi: 10.18097/jpbmc20115701014
- Blanco E, Andreu D, Sobrino F. Peptide Vaccines Against Foot-and-Mouth Disease Virus. *Curr Res Emerg Trends* (2017), 317–32. doi: 10.21775/9781910190517.13
- Bezu L, Kepp O, Cerrato G, Pol J, Fucikova J, Spisek R, et al. Trial Watch: Peptide-Based Vaccines in Anticancer Therapy. *Oncoimmunology* (2018) 7:e1511506. doi: 10.1080/2162402X.2018.1511506
- Azmi F, Fuaad AAHA, Skwarczynski M, Toth I. Recent Progress in Adjuvant Discovery for Peptide-Based Subunit Vaccines. *Hum Vaccines Immunother* (2014) 10:778–96. doi: 10.4161/hv.27332
- Awate S, Babiuk LA, Mutwiri G. Mechanisms of Action of Adjuvants. *Front Immunol* (2013) 4:1–10. doi: 10.3389/fimmu.2013.00114
- Chattopadhyay S, Chen JY, Chen HW, Jack Hu CM. Nanoparticle Vaccines Adopting Virus-Like Features for Enhanced Immune Potentiation. *Nanotheranostics* (2017) 1:244–60. doi: 10.7150/ntno.19796
- Gregory AE, Titball R, Williamson D. Vaccine Delivery Using Nanoparticles. *Front Cell Infect Microbiol* (2013) 3:13. doi: 10.3389/fcimb.2013.00013
- Peek LJ, Middaugh CR, Berkland C. Nanotechnology in Vaccine Delivery. *Adv Drug Deliv Rev* (2008) 60:915–28. doi: 10.1016/j.addr.2007.05.017
- Gheibi Hayat SM, Darroudi M. Nanovaccine: A Novel Approach in Immunization. *J Cell Physiol* (2019) 234:12530–6. doi: 10.1002/jcp.28120
- Zhao L, Seth A, Wibowo N, Zhao C-XX, Mitter N, Yu C, et al. Nanoparticle Vaccines. *Vaccine* (2014) 32:327–37. doi: 10.1016/j.vaccine.2013.11.069
- Fenollosa R, Garcia-Rico E, Alvarez S, Alvarez R, Yu X, Rodriguez I, et al. Silicon Particles as Trojan Horses for Potential Cancer Therapy. *J Nanobiotechnol* (2014) 12:1–10. doi: 10.1186/s12951-014-0035-7
- Rivera Gil P, Hühn D, del Mercato LL, Sasse D, Parak WJ. Nanopharmacy: Inorganic Nanoscale Devices as Vectors and Active Compounds. *Pharmacol Res* (2010) 62:115–25. doi: 10.1016/j.phrs.2010.01.009
- Taki A, Smooker P. Small Wonders—The Use of Nanoparticles for Delivering Antigen. *Vaccines* (2015) 3:638–61. doi: 10.3390/vaccines3030638
- Yang Y, Bernardi S, Song H, Zhang J, Yu M, Reid JC, et al. Anion Assisted Synthesis of Large Pore Hollow Dendritic Mesoporous Organosilica Nanoparticles: Understanding the Composition Gradient. *Chem Mater* (2016) 28:704–7. doi: 10.1021/acs.chemmater.5b03963
- Lu Y, Yang Y, Gu Z, Zhang J, Song H, Xiang G, et al. Glutathione-Depletion Mesoporous Organosilica Nanoparticles as a Self-Adjuvant and Co-delivery Platform for Enhanced Cancer Immunotherapy. *Biomaterials* (2018) 175:82–92. doi: 10.1016/j.biomaterials.2018.05.025
- Cha BG, Jeong JH, Kim J. Extra-Large Pore Mesoporous Silica Nanoparticles Enabling Co-Delivery of High Amounts of Protein Antigen and Toll-Like Receptor 9 Agonist for Enhanced Cancer Vaccine Efficacy. *ACS Cent Sci* (2018) 4:484–92. doi: 10.1021/acscentsci.8b00035
- Shen D, Yang J, Li X, Zhou L, Zhang R, Li W, et al. Biphasic Stratification Approach to Three-Dimensional Dendritic Biodegradable Mesoporous Silica Nanospheres. *Nano Lett* (2014) 14:923–32. doi: 10.1021/nl404316v
- Mody KT, Popat A, Mahony D, Cavallaro AS, Yu C, Mitter N. Mesoporous Silica Nanoparticles as Antigen Carriers and Adjuvants for Vaccine Delivery. *Nanoscale* (2013) 5:5167–79. doi: 10.1039/c3nr00357d
- Xu C, Lei C, Yu C. Mesoporous Silica Nanoparticles for Protein Protection and Delivery. *Front Chem* (2019) 7:290. doi: 10.3389/fchem.2019.00290
- Manolova V, Flace A, Bauer M, Schwarz K, Saudan P, Bachmann MF. Nanoparticles Target Distinct Dendritic Cell Populations According to Their Size. *Eur J Immunol* (2008) 38:1404–13. doi: 10.1002/eji.200737984

24. Bachmann MF, Jennings GT. Vaccine Delivery: A Matter of Size, Geometry, Kinetics and Molecular Patterns. *Nat Rev Immunol* (2010) 10:787–96. doi: 10.1038/nri2868
25. Reddy ST, van der Vlies AJ, Simeoni E, Angeli V, Randolph GJ, O'Neil CP, et al. Exploiting Lymphatic Transport and Complement Activation in Nanoparticle Vaccines. *Nat Biotechnol* (2007) 25:1159–64. doi: 10.1038/nbt1332
26. de Pádua Oliveira DC, de Barros ALB, Belardi RM, de Goes AM, de Oliveira Souza BK, Soares DCF. Mesoporous Silica Nanoparticles as a Potential Vaccine Adjuvant Against Schistosoma Mansoni. *J Drug Deliv Sci Technol* (2016) 35:234–40. doi: 10.1016/j.jddst.2016.07.002
27. Virginio VG, Bandeira NC, Leal FMDA, Lancellotti M, Zaha A, Ferreira HB. Assessment of the Adjuvant Activity of Mesoporous Silica Nanoparticles in Recombinant Mycoplasma Hypopneumoniae Antigen Vaccines. *Heliyon* (2017) 3(1):e00225. doi: 10.1016/j.heliyon.2016.E00225
28. Zhao L, Mahony D, Cavallaro AS, Zhang B, Zhang J, Deringer JR, et al. Immunogenicity of Outer Membrane Proteins VirB9-1 and VirB9-2, A Novel Nanovaccine Against Anaplasma Marginale. *PLoS One* (2016) 11:e0154295. doi: 10.1371/journal.pone.0154295
29. Bai M, Dong H, Su X, Jin Y, Sun S, Zhang Y, et al. Hollow Mesoporous Silica Nanoparticles as Delivery Vehicle of Foot-and-Mouth Disease Virus-Like Particles Induce Persistent Immune Responses in Guinea Pigs. *J Med Virol* (2019) 91:941–8. doi: 10.1002/jmv.25417
30. Blanco E, Cubillos C, Moreno N, Bárcena J, de la Torre BG, Andreu D, et al. B Epitope Multiplicity and B/T Epitope Orientation Influence Immunogenicity of Foot-and-Mouth Disease Peptide Vaccines. *Clin Dev Immunol* (2013) 2013. doi: 10.1155/2013/475960
31. Blanco E, Guerra B, de la Torre BG, Defaus S, Dekker A, Andreu D, et al. Full Protection of Swine Against Foot-and-Mouth Disease by a Bivalent B-Cell Epitope Dendrimer Peptide. *Antiviral Res* (2016) 129:74–80. doi: 10.1016/j.antiviral.2016.03.005
32. de León P, Cañas-Arranz R, Defaus S, Torres E, Forner M, Bustos MJ, et al. Swine T-Cells and Specific Antibodies Evoked by Peptide Dendrimers Displaying Different FMDV T-Cell Epitopes. *Front Immunol* (2021) 11:621537. doi: 10.3389/fimmu.2020.621537
33. Defaus S, Forner M, Cañas-Arranz R, de León P, Bustos MJ, Rodríguez-Pulido M, et al. Designing Functionally Versatile, Highly Immunogenic Peptide-Based Multi-epitopic Vaccines Against Foot-and-Mouth Disease Virus. *Vaccines (Basel)* (2020) 8(3):406. doi: 10.3390/vaccines8030406
34. Wu Y, Ellis RD, Shaffer D, Fontes E, Malkin EM, Mahanty S, et al. Phase 1 Trial of Malaria Transmission Blocking Vaccine Candidates Pfs25 and Pvs 25 Formulated With Montanide ISA 51. *PLoS One* (2008) 3(7):e2636. doi: 10.1371/journal.pone.0002636
35. Reed SG, Bertholet S, Coler RN, Friede M. New Horizons in Adjuvants for Vaccine Development. *Trends Immunol* (2009) 30:23–32. doi: 10.1016/j.it.2008.09.006
36. Lin YS, Haynes CL. Synthesis and Characterization of Biocompatible and Size-Tunable Multifunctional Porous Silica Nanoparticles. *Chem Mater* (2009) 21:3979–86. doi: 10.1021/cm901259n
37. Patwardhan SV, Emami FS, Berry RJ, Jones SE, Naik RR, Deschaume O, et al. Chemistry of Aqueous Silica Nanoparticle Surfaces and the Mechanism of Selective Peptide Adsorption. *J Am Chem Soc* (2012) 134(14):6244–56. doi: 10.1021/ja211307u
38. Rivera-Gil P, Jimenez De Aberasturi D, Wulf V, Pelaz B, Del Pino P, Zhao Y, et al. The Challenge to Relate the Physicochemical Properties of Colloidal Nanoparticles to Their Cytotoxicity. *Acc Chem Res* (2013) 46:743–9. doi: 10.1021/ar300039j
39. Schweiger C, Hartmann R, Zhang F, Parak WJ, Kissel TH, Rivera-Gil P. Quantification of the Internalization Patterns of Superparamagnetic Iron Oxide Nanoparticles With Opposite Charge. *J Nanobiotechnol* (2012) 10:28. doi: 10.1186/1477-3155-10-28
40. Zamora-Perez P, Tsoutsis D, Xu R, Rivera-Gil P. Hyperspectral-Enhanced Dark Field Microscopy for Single and Collective Nanoparticle Characterization in Biological Environments. *Mater (Basel)* (2018) 11(2):243. doi: 10.3390/ma11020243
41. Mahmoudi M, Meng J, Xue X, Liang XJ, Rahman M, Pfeiffer C, et al. Interaction of Stable Colloidal Nanoparticles With Cellular Membranes. *Biotechnol Adv* (2014) 32:679–92. doi: 10.1016/j.biotechadv.2013.11.012
42. Chanana M, Rivera-Gil P, Correa-Duarte MA, Liz-Marzán LM, Parak WJ. Physicochemical Properties of Protein-Coated Gold Nanoparticles in Biological Fluids and Cells Before and After Proteolytic Digestion. *Angew. Chemie - Int Ed* (2013) 52:4179–83. doi: 10.1002/anie.201208019
43. Bros M, Nuhn L, Simon J, Moll L, Mailänder V, Landfester K, et al. The Protein Corona as a Confounding Variable of Nanoparticle-Mediated Targeted Vaccine Delivery. *Front Immunol* (2018) 9:1760. doi: 10.3389/fimmu.2018.01760
44. Ge C, Tian J, Zhao Y, Chen C, Zhou R, Chai Z. Towards Understanding of Nanoparticle-Protein Corona. *Arch Toxicol* (2015) 89:519–39. doi: 10.1007/s00204-015-1458-0
45. Ozboyaci M, Kokh DB, Corni S, Wade RC. Modeling and Simulation of Protein-Surface Interactions: Achievements and Challenges. *Q Rev Biophys* 49 (2016) 49:e4. doi: 10.1017/S0033583515000256
46. Ge C, Du J, Zhao L, Wang L, Liu Y, Li D, et al. Binding of Blood Proteins to Carbon Nanotubes Reduces Cytotoxicity. *Proc Natl Acad Sci USA* (2011) 108:16968–73. doi: 10.1073/pnas.1105270108
47. Hartley JW, Evans LH, Green KY, Naghashfar Z, Macias AR, Zerfas PM, et al. Expression of Infectious Murine Leukemia Viruses by RAW264.7 Cells, a Potential Complication for Studies With a Widely Used Mouse Macrophage Cell Line. *Retrovirology* (2008) 5:6–11. doi: 10.1186/1742-4690-5-1
48. Berghaus LJ, Moore JN, Hurley DJ, Vandenplas ML, Fortes BP, Wolfert MA, et al. Innate Immune Responses of Primary Murine Macrophage-Lineage Cells and RAW 264.7 Cells to Ligands of Toll-Like Receptors 2, 3, and 4. *Comp Immunol Microbiol Infect Dis* (2010) 33:443–54. doi: 10.1016/j.cimid.2009.07.001
49. Kastl R, Sasse D, Wulf V, Hartmann R, Mircheski J, Ranke C, et al. Multiple Internalization Pathways of Polyelectrolyte Multilayer Capsules Into Mammalian Cells. *ACS Nano* (2013) 7:6605–18. doi: 10.1021/nn306032k
50. Assanga I. Cell Growth Curves for Different Cell Lines and Their Relationship With Biological Activities. *Int J Biotechnol Mol Biol Res* (2013) 4:60–70. doi: 10.5897/ijbmr2013.0154
51. Demento SL, Cui W, Criscione JM, Stern E, Tulipan J, Kaech SM, et al. Role of Sustained Antigen Release From Nanoparticle Vaccines in Shaping the T Cell Memory Phenotype. *Biomaterials* (2012) 33:4957–64. doi: 10.1016/j.biomaterials.2012.03.041
52. Men Y, Gander B, Merkle HP, Corradin G. Induction of Sustained and Elevated Immune Responses to Weakly Immunogenic Synthetic Malarial Peptides by Encapsulation in Biodegradable Polymer Microspheres. *Vaccine* (1996) 14:1442–50. doi: 10.1016/S0264-410X(96)00074-6
53. Liu T, Li L, Teng X, Huang X, Liu H, Chen D, et al. Single and Repeated Dose Toxicity of Mesoporous Hollow Silica Nanoparticles in Intravenously Exposed Mice. *Biomaterials* (2011) 32:1657–68. doi: 10.1016/j.biomaterials.2010.10.035
54. Fu C, Liu T, Li L, Liu H, Chen D, Tang F. The Absorption, Distribution, Excretion and Toxicity of Mesoporous Silica Nanoparticles in Mice Following Different Exposure Routes. *Biomaterials* (2013) 34:2565–75. doi: 10.1016/j.biomaterials.2012.12.043
55. He X, Nie H, Wang K, Tan W, Wu X, Zhang P. In Vivo Study of Biodistribution and Urinary Excretion of Surface-Modified Silica Nanoparticles. *Anal Chem* (2008) 80:9597–603. doi: 10.1021/ac801882g
56. He Q, Zhang Z, Gao F, Li Y, Shi J. In Vivo Biodistribution and Urinary Excretion of Mesoporous Silica Nanoparticles: Effects of Particle Size and Pegylation. *Small* (2011) 7:271–80. doi: 10.1002/smll.201001459
57. Toda T, Yoshino S. Enhancement of Ovalbumin-Specific Th1, Th2, and Th17 Immune Responses by Amorphous Silica Nanoparticles. *Int J Immunopathol Pharmacol* (2016) 29:408–20. doi: 10.1177/0394632016656192
58. An M, Li M, Xi J, Liu H. Silica Nanoparticle as a Lymph Node Targeting Platform for Vaccine Delivery. *ACS Appl Mater Interfaces* (2017) 9:23466–75. doi: 10.1021/acsami.7b06024

Conflict of Interest: The authors declare that the research was conducted in the absence of any commercial or financial relationships that could be construed as a potential conflict of interest.

Copyright © 2021 An, Defaus, Andreu and Rivera-Gil. This is an open-access article distributed under the terms of the Creative Commons Attribution License (CC BY). The use, distribution or reproduction in other forums is permitted, provided the original author(s) and the copyright owner(s) are credited and that the original publication in this journal is cited, in accordance with accepted academic practice. No use, distribution or reproduction is permitted which does not comply with these terms.